Hindawi Publishing Corporation
ISRN Renewable Energy
Volume 2013, Article ID 480137, 8 pages
http://dx.doi.org/10.1155/2013/480137

Research Article

Modeling Solar Energy Transfer through Roof Material in Africa Sub-Saharan Regions

Julien G. Adounkpe,[1] A. Emmanuel Lawin,[2] Clément Ahouannou,[3] Rufin Offin Lié Akiyo,[4] and Brice A. Sinsin[1]

[1] *Laboratory of Applied Ecology, Faculty of Agronomic Sciences, University of Abomey Calavi, 03 BP 3908 Cotonou, Benin*
[2] *Laboratory of Applied Hydrology, Faculty of Sciences and Technologies, University of Abomey Calavi UAC, BP 526, Benin*
[3] *Laboratory of Applied Energetic and Mechanics Ecole Polytechnique d'Abomey Calavi, University of Abomey Calavi, 03P 1175 Cotonou, Benin*
[4] *Department of Geography, University of Parakou, BP 123, Benin*

Correspondence should be addressed to Julien G. Adounkpe; julvictoire@yahoo.com

Received 29 July 2013; Accepted 28 August 2013

Academic Editors: F. E. Little and M. Souliotis

As a result of the global warming, the atmospheric temperature in sub-Saharan regions of Africa may drastically increase, thus worsening the poor living conditions already experienced by people in those regions. Roof's thermal insulation capacity may play key role in reducing indoor thermal comfort cost. In the present study, effort is put to model heat transfer through roofs in south Saharan regions. Validation of the model was achieved using the slightly sloppy galvanized aluminum-iron sheet roof. Atmospheric data were hourly measured during April and June in Ouagadougou, Burkina Faso. Solar energy values increase from $24.50 \pm 0.50\ W/m^2$ in the morning to a maximum of $900.1 \pm 0.8\ W/m^2$ in the early afternoon. Ambient temperature follows the same trend as solar radiation with a maximum at $40.0 \pm 0.2^{\circ}C$. Wind speed varies from 0.5 to 4.0 ± 0.1 m/s. The measured roof inner wall temperatures agreed excellently with the developed model with a Nash-Sutcliffe Coefficient of Efficiency of 0.988. Energy flux entering the room through the roof varies from $63.1 \pm 0.3\ W/m^2$ earlier in the morning to a maximum of $115.3 \pm 0.5\ W/m^2$ in the earlier afternoon. These results shall help to better design human habitat under changing climate conditions in the sub-Saharan regions.

1. Introduction

Ever since the appearance of human beings on earth, beside food and other basic needs, shelters, or dwelling places have been of major preoccupation. Human beings have set up their homes utilizing materials from the nature. To protect themselves from rain, heat, wind, cold, snows, or any sort of enemies, human beings have invented, at very early ages, habitat which has evolved from the caves, natural physical dwellings to the modern houses known today [1]. One of the most important elements of a house is its roof. Indeed, in sub-Saharan countries and most countries on the earth, roof must stand rainy seasons and during periods of elevated heat must provide certain comfort [2]. The effectiveness of the roof in terms of comfort and sustainability requires the thermal insulation capacity and the mechanical strength of materials employed.

The shapes of roof are adapted to the type of climate of a given region [3]. Over the world, there are more than 30 types of roof [4]. Moreover, many factors contribute to the differences among the types of roof. The most important factors are the technology, the materials, the environment, and the mere habit [4]. For instance, plat roof dominates in dry regions, while cone shape roof dominates in semi-dry regions such as some parts of Africa. Short eaves gable roof type is widely observed both in Europe and North America, while deep eaves are dominant in Masson Asia [4].

Over ages, as human shelters, roofs have evolved from what was then called traditional roofing to what is known nowadays to be the modern roofing. In most sub-Saharan

countries, traditional roofing is still at use most importantly in rural areas.

Traditional roofs made of indigenous or local materials such as woods for stands or frames and straws (Figure 1), leaves or herbs, and so forth, for covertures, have thermal isolation properties. Their main drawback is their relatively short life which forces the users to rebuild basically almost after every rainy season [2].

Modern roofs are made of metal sheets (Figure 2), reinforced concrete, and so forth. Iron, aluminum, and zinc, most often protected against wear are used as roof coverings and have mechanical resistances characterized by their relatively long life. Galvanized iron sheet finds use in developing world, basically where high rainfall is registered annually [5]. The main handicap of the modern roofing is their low isolation capacity.

In the light of climate change and all its adverse effects and giving the fact that increasing number of houses are adopting the modern roofing along with high thermal comfort cost, combining traditional roofing and modern roofing at one hand and modifying modern existing roofs on the other hand to get indoor comfort at an affordable cost are of interest [6].

Green or vegetative roofs are in use in several European and American countries [7]. Several problems, notably the thermal isolation leading to the reduced energy consumption and energy conservation [8] and noise reduction, are solved by green roofing [9]. However, those benefits linked to green roofs are more significant for extremely compact tropical cities with severe shortage of ground-level green spaces and intense Urban Heat Island effects [10, 11].

Moreover, green roofing is not much in use in south Saharan regions for several reasons. First, those regions have no space problem, and there are few compact cities where such a technique could be deployed. Second, the construction and the maintenance costs of those green roofing are way beyond what people in those regions could bear.

Climate change is a challenging situation to human habitat as far as their thermal comfort in houses. In a dry and hot climate of Mexicali in Mexico, a city of same climate characteristics as Ougagougou where the present study was conducted, a field study was done, consisting on the determination of electrical energy consumption of low income dwellers and their perception of thermal comfort in accordance with the design and the building material [12].

Sustainable buildings have been designed by architects for the improvement of indoor environmental quality, basically including the provision of comfortable temperatures and humidities. The users' perceptions of thermal comfort had been surveyed in 36 sustainable commercial and institutional buildings in 11 countries [13]. The focus of those studies among others was the overall thermal comfort in buildings. However, few studies deal with the specific thermal contribution of the roof to the house. The possibility of roof light for indoor comfort was explored in order to design an innovative roofing system for the tropics with plenty of sunshine and high humidity [14].

In recent years, great interests have been noticed in the field of solar radiation modeling. Models have been developed to evaluate both global and diffuse solar radiations. Employing a sensor FLA613-GS that gives direct current proportional to global radiation, the global solar radiance was evaluated [15]. In 2011, an estimation of diffuse solar radiation on horizontal plane was performed in three cities of Nigeria in west Africa. Correlation between the clearance index and the diffuse to global solar radiation ratio was employed in the estimation of the diffuse radiation. The model efficiency is proven worldwide according to the authors [16]. Furthermore, real time monitoring of global solar radiation was achieved designing a model of TCP/IP with an embedded internet based data acquisition system [17]. Even though scientists in the field of solar energy have developed models to monitor solar radiation, in the literature, to the best of our knowledge, it was not possible to see effort related to roof modeling linked to solar energy in the south Saharan region of Africa.

Figure 1: Traditional roofing in South Sahara Africa. The roof cover is made of straws and needs to be renewed after each rainy season.

Figure 2: Typical modern roof type in Sub-Sahara Africa. Most of the roofs are made of metal sheets, basically iron sheet with slight slope and oriented south.

The present study aims at modeling heat transfer through roofs in sub-Saharan region in order to predict the roof contribution to the overall heat of the room and to select roof materials that lower comfort cost in those regions where about 70% of the room overall heat comes from the roof [18].

2. The Roof Thermal Model

As it is known, a model is meant to be the simplest way of looking at a complex phenomenon. The conceptualization of

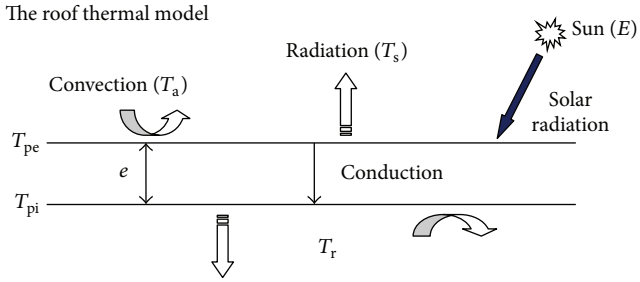

FIGURE 3: Model of heat flux exchanged between the roof and its surroundings, where e = thick of the sheet or roof, T_r = temperature of the room, T_a = ambient temperature, T_s = temperature of the sky, T_{pe} = the roof outer wall temperature, T_{pi} = the roof inner wall temperature, and E = solar radiation.

the heat flux through the roof of a house can be expressed as follows (Figure 3):

$$\varphi = \text{incoming flux} - \text{out going flux}$$
$$\varphi = \frac{\lambda}{e}\left(T_{pe} - T_{pi}\right), \tag{1}$$

where:

φ is the heat flux through the roof,

λ, the thermal conductivity of the sheet (roof),

e is the thick of the sheet,

T_{pe} and T_{pi} the external and internal wall temperature, respectively.

In fact, T_{pe} and T_{pi} are obtained through studious mathematical calculations that require an energy balance to be established at the interfaces atmosphere-roof and roof-room.

A roof exposed to the solar radiation E is the center of three modes of heat transfer: conduction, convection, and radiation.

When there is between two bodies a temperature gradient, heat travels from the hotter to the colder; thus the difference tends to resolve spontaneously. Essentially transfers between two bodies implement three distinct processes, simultaneous or not: conduction, convection, and radiation.

2.1. Conduction. Two bodies at different temperatures brought into contact exchange heat by conduction where the heat flows from the hottest to the coldest. In the case of the present study, heat flows within the roof body from the outer wall to the inner wall of the roof due to the temperature gradient between the external and the internal walls of the roof.

2.2. Convection. When a body and a fluid (water, air, etc.), at different temperatures, are in contact, there is heat exchange by forced convection (when the speed of circulation of the fluid is imposed) or natural (otherwise).

2.3. Radiation. Any living or inanimate object whose temperature is above absolute zero (−273.15°C) emits electromagnetic radiations that carry a certain amount of energy. Two remote objects exchange heat by emission or radiation. The sun is object of such a radiation towards the earth and the other planets.

A roof exposed to the solar radiation is the center of thermal exchanges characterized by the following thermal coefficients.

(i) Coefficient of Thermal Conductivity λ. It represents the amount of heat which passes through the body per meter in a second for a temperature difference of 1°C. Its unit is W/m/°C.

A material will be more heat conductor as its coefficient of thermal conductivity is high.

(ii) Absorption Coefficient ε_{po}. It represents the fraction of solar radiation absorbed by the roof. ε_{po} is unitless.

(iii) Emissivity. The roof has the property of emitting part of radiation received towards the sky and towards the room characterized, respectively, by emissivity coefficients ε_e and ε_i. These coefficients characterize the radiation in the infrared.

(iv) Coefficient of Convection h. It characterizes the heat exchange and represents the flow per unit area of contact and degree ($W/m^2/°C$). h_i for internal convection, and h_e for external convection.

2.4. Adjacent Fluids to the Roof. At both sides of the roof, there is heat exchange between the roof and the room air and the atmospheric air characterized by physical parameters (λ_e, C_{pe}, ρ_e, μ_e), and a flow velocity.

3. Energetic Balance of the Roof

The roof exchanges heat with its surroundings as it receives solar radiation E.

(i) At the Roof External Wall. Consider

$$\varphi_{abs} = \varepsilon_e \cdot E,$$
$$\varphi_{lost,conv\_e} = h_e \cdot \left(T_{pe} - T_a\right), \tag{2}$$
$$\varphi_{lost,rad\_e} = \sigma \cdot \varepsilon_e \cdot \left(T_{pe}^4 - T_S^4\right).$$

(ii) Heat Recovered from the Roof (Material) by Conduction. Consider

$$\varphi_{cond} = \frac{\lambda}{e} \cdot \left(T_{pe} - T_{pi}\right). \tag{3}$$

(iii) At the Roof Internal Wall. Consider

$$\varphi_{lost,conv\_i} = h_i \cdot \left(T_{pi} - T_{room}\right),$$
$$\varphi_{lost,rad\_i} = \sigma \cdot \varepsilon_i \cdot S \cdot \left(T_{pi}^4 - T_{room}^4\right). \tag{4}$$

(iv) Heat Balance on the Roof. One has

$$\varphi_e = \varphi_{\text{abs}} = \varphi_{\text{lost,conv\_}e} + \varphi_{\text{lost,rad\_}e} + \varphi_{\text{cond}}, \tag{5}$$

$$\varepsilon_e \cdot E = \left[h_e \cdot \left(T_{\text{pe}} - T_{\text{a}}\right) + \sigma \cdot \varepsilon_e \cdot \left(T_{\text{pe}}^4 - T_{\text{S}}^4\right) + \frac{\lambda}{e} \cdot \left(T_{\text{pe}} - T_{\text{pi}}\right) \right], \tag{6}$$

$$\varphi_s = \varphi_{\text{recover\_room}} = \varphi_g + \left(\varphi_{\text{lost,conv\_}i} + \varphi_{\text{lost,rad\_}i}\right). \tag{7}$$

Knowing that $\varphi_g = O$,

$$\varphi_{\text{recover\_room}} = \varphi_{\text{cond}} = \varphi_{\text{lost,conv\_}i} + \varphi_{\text{lost,rad\_}i}, \tag{8}$$

$$\frac{\lambda}{e} \cdot \left(T_{\text{pe}} - T_{\text{pi}}\right) = \left[h_i \cdot \left(T_{\text{pi}} - T_{\text{room}}\right) + \sigma \cdot \varepsilon_i \cdot \left(T_{\text{pi}}^4 - T_{\text{room}}^4\right) \right]. \tag{9}$$

Combining (6) and (9) leads to the system of two equations where the unknowns are T_{pe} and T_{pi}; both are raised to power 1 and 4:

$$\varepsilon_e \cdot E = \left[h_e \cdot \left(T_{\text{pe}} - T_{\text{a}}\right) + \sigma \cdot \varepsilon_e \cdot \left(T_{\text{pe}}^4 - T_{\text{S}}^4\right) + \frac{\lambda}{e} \cdot \left(T_{\text{pe}} - T_{\text{pi}}\right) \right],$$

$$\frac{\lambda}{e} \cdot \left(T_{\text{pe}} - T_{\text{pi}}\right) = \left[h_i \cdot \left(T_{\text{pi}} - T_{\text{room}}\right) + \sigma \cdot \varepsilon_i \cdot \left(T_{\text{pe}}^4 - T_{\text{room}}^4\right) \right]. \tag{10}$$

3.1. Modeling h_e. h_e is the external convection coefficient between the outside ambient air and the roof. We made the assumption that this exchange is governed by forced convection because for simplicity, the external wind speed is maintained constant for a defined time slot. Thus the following formulas were used to evaluate

$$h_e = 5.7 + 3.8V \quad \text{for } V \le 4\,\text{m/s}, \qquad h_e = 7.5V^{0.8} \quad \text{for } V > 4\,\text{m/s}, \tag{11}$$

where V is the velocity of the wind.

3.2. Modeling h_i. The roof internal side exchanges heat with the room by natural convection with air inside the room with hi which is the convection coefficient given by

$$h_i = \frac{\left(\text{Nu} \cdot \lambda_e\right)}{L}, \tag{12}$$

where Nu is Nusselt number, L is length of the roof and λ_e is thermal conductivity of the air. Out of these three parameters, only L can be easily known. The Nusselt number value is given by the correlation:

$$\text{Nu} = (\text{Gr} \cdot \text{Pr})^m, \tag{13}$$

where Gr is Grashof number, Pr is Prandtl number, and A and m are constants. Pr and Gr given for air are, respectively, Pr ≈ 0.7, and Grashof number can be calculed by

$$\text{Gr} = \frac{\beta g \Delta\theta \rho_e^2 L_3}{\mu_e^2}, \tag{14}$$

where β is the inverse of the average temperature of the air film, $\Delta\theta$ is temperature difference between the air film and the roof internal wall, λ_e is thermal conductivity of the air, ρ_e is density of air film (Kg·m^{-3}), μ_e is dynamic viscosity of the air (N·m^{-2}·S^{-1}), and $g = 9.81\,\text{m/s}^2$ is gravity intensity.

λ_e, ρ_e, and μ_e are tabulated values of the air for a given air temperature film work. For the convenience of the numerization, the air characteristics were linearized, and the relationships found are directly used in the program.

3.3. Modeling λ_e, ρ_e, and μ_e. Here we give the linear relationships obtained after linear regression in regression domains quite correct ($r \to 1, -1, -0.99, 0.99$) (in Kg/m^3):

$$\lambda_e = \begin{cases} 18.25 \times 10^{-4} + 81.5 \times 10^{-6} T; & \text{for } 200 \le T < 300 \\ 35.00 \times 10^{-4} + 75.8 \times 10^{-6} T; & \text{for } 300 \le T < 350 \\ 46.90 \times 10^{-4} + 72.4 \times 10^{-6} T; & \text{for } 350 \le T \le 400, \end{cases}$$

$$\rho_e = \begin{cases} 2,9300 - 59,10 \times 10^{-4} T; & \text{for } 200 \le T < 300 \\ 2,2583 - 35,88 \times 10^{-4} T; & \text{for } 300 \le T < 350 \\ 1,8058 - 23,08 \times 10^{-4} T; & \text{for } 350 \le T \le 400, \end{cases}$$

$$\mu_e = \begin{cases} 29.81 \times 10^{-7} + 51.73 \times 10^{-9} T; & \text{for } 200 \le T < 300 \\ 47.34 \times 10^{-7} + 45.76 \times 10^{-9} T; & \text{for } 300 \le T < 350 \\ 59.80 \times 10^{-7} + 42.2 \times 10^{-9} T; & \text{for } 350 \le T \le 400, \end{cases} \tag{15}$$

where T (in K) is the temperature of the air film estimated at $T = T_{\text{r}} + 10$ during day time and $T = T_{\text{r}} - 5$ at night.

3.4. Modeling T_s, the Temperature of the Sky. Estimation of the temperature of the sky can be achieved through three different formulae depending on the atmospheric conditions:

$$T_{\text{s}} = T_{\text{a}} - 12 \quad \text{or} \quad T_{\text{s}} = \varepsilon {T_{\text{a}}}^{1/4}. \tag{16}$$

ε is emissivity of the sky which can take two forms:

$$\varepsilon = 1 - 0.161 \cdot \exp\left[-0.00077\left(T_{\text{a}} - 273\right)\right]^2 \quad \text{or } \varepsilon = 0.787 - 0.764 \ln\left(\frac{T_{\text{v}}}{273}\right), \tag{17}$$

where T_{v} is the vapor temperature.

Of those three formulas, the second one was found to fit the best the overall model taking into account the level of

error acceptability. Hence, to evaluate the temperature of the sky the present model uses the following T_s equation:

$$T_s = \left[1 - 0.161 \cdot \exp\left[-0.00077\left(T_a - 273\right)\right]^2\right] T_a{}^{1/4}. \quad (18)$$

4. Method and Material

4.1. Study Area

4.1.1. Climate. The study was conducted near the University of Ougadougou, Ouagadougou, Burkina Faso, a city known to be located in the Soudano-Sahelian zone. The climate is characterized by a unimodal precipitation regime, with a rainfall of about 600 mm per year. Rainfall events are mainly generated by the dynamic of the West African Monsoon (WAM). The rainy season stretches from mid-May to mid-October, with an average temperature of 30°C. But the key period is known to be June-July-August-September (JJAS) which totalized more than 80% of the seasonal rainfall. The cold season runs from December to January, with a minimum temperature of 19°C. The maximum temperature during the hot season, which runs from March to May, can reach 45°C. The harmattan, a dry and cold wind, from late November to mid-February, blows north-east with a high temperature gradient between daytime and night that can reach. Relative air humidity varies from 20% in March during dry season to 80% in August during rainy season with a mean of 49% [19]. This provides thermal comfort even with high temperatures.

4.1.2. Study Sites. The study was undertaken at a site located inside the campus of the University of Ouagadougou where the study materials were installed. The geographic characteristics of the site are as follows: 12°22′46.19″N, 1°29′58.77″O, and elevation 295 m.

4.2. Material.

The experimental boxes are made of wood on top of which galvanized iron sheets cover is placed to serve as the roof. The boxes were put at a height of 1 m above the ground at points where no influence from building shade, trees, or other can affect the measurements.

4.3. Solar Radiation Measurement.

For the solar radiation measurement, several equipments are available depending on the type of solar radiation of interest, either global, diffuse, or direct. Global solar radiation is the sum of the direct and the diffuse. The versatile CM-11 pyranometer was used to measure the global radiation in Finland, Estonia, Poland, and Sweden, the pyranometer PP-1 for the diffuse one, and the actinometer AT-50 for the direct solar radiation in Latvia and Lithuania [20]. Those are very high technology that was not available to us at the moment of the experimentation. However, we used a CMP-pyranometer that fulfils the requirements of IEC 61215 and IEC 60904-X for the accurate measurement of irradiance for photovoltaic and thermal solar devices. That pyranometer was used as reference instruments to test and certify PV cells for power plant projects. It was proven very accurately and efficient. That instrument was placed close to the box at the same height from the ground.

Table 1: Solar radiation SR (W/m^2), wind speed V (m/s) and ambient temperature are recorded on an hourly basis.

Time	Solar radiation (E)	Wind speed (V m/s)	Ambient temperature (T_a °C)
7:00	130.0	1.0	27.5
8:00	354.2	2.0	31.7
9:00	630.7	3.0	33.9
10:00	775.9	3.0	35.7
11:00	853.3	3.0	37.4
12:00	900.1	3.0	38.4
13:00	848.1	2.0	39.7
14:00	751.9	2.0	40.0
15:00	572.2	2.0	40.5
16:00	339.3	2.0	39.9
17:00	106.2	2.0	39.2
18:00	17.5	2.0	37.0

4.4. Temperature Gauges.

Temperature gauges were positioned everywhere needed: the ambient temperature, the room temperature, the external and internal roof wall temperatures, and so forth. The ambient temperature is measured at a height of 5 m above the ground. The gauges were electrically connected to the temperature sensor that gives a simultaneous read-out of all temperatures with decimal absolute error.

4.5. Wind Speed Measurement.

Two main types of instruments that measure wind speed are the rotating cup anemometer and the propeller anemometer. Both types of anemometers consist of two subassemblies, the sensor and the transducer. The sensor is the device that rotates by the force of the wind. The transducer is the device that generates the signal suitable for recording. Most of the time, the signal needs to be conditioned by signal conditioner and displayed by loggers and recorder. In the present study, the rotating cup anemometer was employed.

5. Results and Discussion

The atmospheric parameters recorded were solar irradiation, wind speed, and ambient temperature. Those parameters were recorded hourly during April and June, on clear sky days. A typical set of measurements is reported in Table 1.

It is very important to understand that the measurements were done on a regular basis of one hour interval for 24 hours a day. The data shown in Table 1 and the following are just an extraction of the one for which solar energy was not null, and that the solar influence can be observed on the temperatures. In fact from 7 p.m. to 6 a.m., solar radiation was zero.

The bands between 15° and 35° north and south around the earth receive the greatest amount of solar energy [21], but the equatorial belt between 15°N and 15°S latitude is the most irradiated. Burkina Faso, Mali, Niger, and the northern part of Benin, Togo, and Nigeria in West Africa are located in

Table 2: Ambient temperature (T_a), solar irradiance (SR), wind speed (V) and the galvanized ion sheet roof room temperature (T_r), the roof inner wall temperature measured (T_{pim}), and simulated (T_{pis}) and energy flux entering the room were reported.

Time (H)	T_a (°C)	SR (W/m^2)	V (m/s)	Al-Fe			
				T_r	T_{pim}	T_{pis}	Flux
8:30	33.0	426.0	2.0	37.4	52.2	49.8	63.1
9:30	33.9	598.0	1.6	41.3	59.9	60.0	96.1
11:00	35.5	840.0	2.0	46.1	64.0	65.4	101.6
12:00	36.8	853.8	2.0	50.3	69.2	71.7	115.3
13:00	38.0	843.0	2.0	51.6	73.0	72.7	115.3
14:00	38.4	715.4	2.5	51.2	65.4	65.8	76.9
15:00	40.1	563.0	2.5	50.1	61.2	61.6	60.0
16:00	39.6	130.0	0.5	44.7	47.3	47.5	13.0
17:00	38.5	114.0	2.0	41.6	42.7	42.9	8.2
18:00	38.0	30.0	2.5	38.6	37.5	38.5	0.0

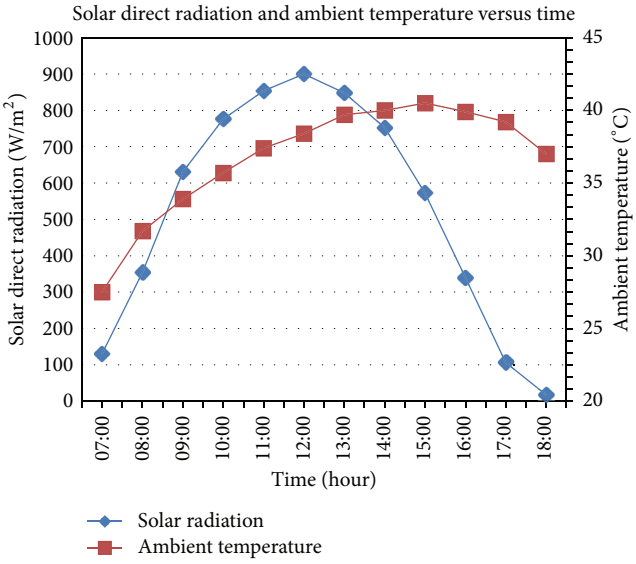

Figure 4: Solar direct radiation (W/m^2) and ambient temperature (°C) recorded at a typical clear sky day of April.

these regions [22]. Consequently, those countries are subject to important solar irradiance and thus have high solar energy potentials.

The solar radiation variation observed and registered in the present study is in accordance with the one observed in various cities of Nigeria [16] and elsewhere [23–25], even though solar irradiance is latitude dependent. At higher latitudes > than 25°, high radiations can be observed as proof of high potential solar energy availability for various solar energy applications. For example, a 5-year cumulative annual global solar radiation was found to be 1693 Kwh/m^2/day in Spain (latitude 42°N, 4.9°W) and 1841 Kwh/m^2/day in Malta (latitude 36°N, 14.5°E) where June and July are the months that receive the greater sunshine [26], giving the proof that solar radiation decreases with the latitude and determines the regional houses architecture [14]. Radiation data recorded at 12 sites around the central part of the Baltic Sea (latitude varies from 54°N, 15°E to 61°N, 24°E) from 1996 to 2000 showed June to be the month of highest solar radiation in most part of the region with an average daily total of 20.9 MJ/m^2 at Visby (57.69°N, 18.35°E) [20]. However, hourly measurements literature data are the ones to compare those of the present study with. Hourly monitoring of ambient temperature, solar global or direct radiation is an important mean for engineers and building designers to select construction materials that correspond to the specific climate. Such reports are rather scarce, while yearly, monthly, and daily mean values are the most reported in the literature [14, 21, 26]. In a study conducted in Ajaccio France, ambient temperature, solar irradiance, wind speed and direction, and so forth were recorded every minute. A perfect relationship between the instantaneous increases of ambient temperature and solar irradiance is observed (Table 2). Both curves, ambient temperature and solar irradiance, well shaped in a Gaussian like form present their respective maximum at about 1:p.m. [25] unlike their counterparts of the present study, where there is a gap of about 2 hours between the maximum of the solar irradiance (1:p.m.) and the ambient temperature (3:p.m.). This can be explained by the presence of dust (fine particles) in the air hindering the ambient air to cool down as the sun is setting, causing a delay of approximately 2 hours between the solar irradiance and the ambient temperature.

Hourly mean temperatures of modern roofs are reported [14]. However, the solar irradiance on which depends the temperature behavior was not reported. Interesting enough, the Gaussian shape was observed and the maximum indoor temperatures for various roofs were reached by 2 p.m. by some roofs and 4 p.m. by others. These results are in line with what we obtained for the validation of the model employing the galvanized iron sheet (Figure 4). The room temperature increases from 37.5°C at 8:30 a.m. to reach a maximum value of 40.1°C by 3:00 p.m. and decreases to 38.0°C by 6:00 p.m. having the same trend as the solar irradiance which increases from 426 W/m^2 by 8:30 a.m. to reach a maximum of 853.8 W/m^2 by noon and decreases to 30 W/m^2. The 2-hours gap between the maximums of the ambient temperature, and the solar irradiance was observed. However, this gap was not observed between the room temperature, the roof inner wall temperature and the solar irradiance. A temperature gradient of about 20°C was observed between the room temperature and the roof inner wall temperature, giving the proof that a substantial gradient of temperature can be achieved if subsequent ceiling was made in buildings.

A similar study conducted [24] shows similar relationships between solar irradiance and ambient temperature where the maximal solar irradiance of 430 W/m^2 attained at 1:00 p.m. shift with the ambient temperature maximum of 46.6°C observed at 2:00 p.m. In contrary, while the room temperature in the present study is quite different from the ambient temperature, the one from [24] observed was similar to the ambient temperature. The difference comes from the ventilation of the room, while in the present, no ventilation

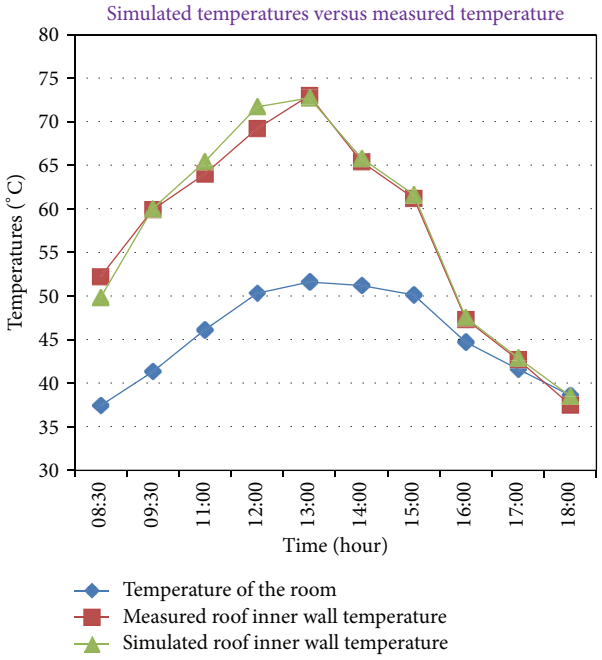

FIGURE 5: This graph shows a perfect agreement between simulated roof inner wall temperatures in green (T_{pis}) and measured roof inner wall temperatures in red (T_{pim}); the temperature of the room is in blue.

is done. As it is known, ventilation reduces temperature. This explains the observed phenomenon.

More importantly, the measured and simulated temperatures of the roof inner temperature were compared. Figure 5 not only shows a gap of 20°C maximum between the roof temperature and the room temperature but also more importantly the similarity between simulated and measured roof inner wall temperatures.

5.1. Model Calibration and Verification for Validation. A model is always a simplification of the complex reality of natural phenomena. This simplification has the merit of both representing the reality in all its extent and keeping accessibility and understandings to those not very well acknowledgeable of the given field. However, the constructed model may not be capable of producing a response that is entirely in line with the behavior of the observed phenomenon [27]. Therefore a model, after being elaborated, needs to be tested with the whole set of data that are available is in short the model needs to be calibrated. The calibration of a model requires that the overall complexity of the mechanism under investigation to be taken into account [28].

For the calibration of the present model, a suitable range of error acceptability has been adopted, after several trials. The linearization of the tabulated temperatures to fill in the software made for the model, the temperature of the air film, the sky temperature, and other parameters in a repeated iterative process were achieved. Even the parameters assumed to be invariant were changed to see how well the model adjusts to them [28].

The verification procedure tests the entire reality of the phenomenon. The final step is the validation which entails a broader set of data and possibly allows comparison with other models dealing with the same observations. Model validation is related to the process of decision making. Thus the current model has been validated and can serve as a successful tool in the hands of experienced acknowledgeable persons in the field.

The qualitative model performance assessment is achieved employing some statistical criteria to compare the data from the measurements and the one produced by the model. These statistical criteria are considered objective and provide unbiased indicators of the model performance [28]. The lower the Mean Absolute Error or the Bias Percentage value, the better the performance of the model. However, the Root Mean Square Error (RMSE) which measures the scatter of the residuals or the Relative Root Mean Square Error which is the normalized RMSE is more expressive than the two others. In our study, the RMSE is calculated using the following formula:

$$\mathrm{RMSE} = \left[\frac{\sum_{i=1}^{N}\left(Q_i^{\mathrm{mod}} - Q_i^{\mathrm{meas}}\right)^2}{N}\right]^{1/2}. \tag{19}$$

The RMSE value computed shows the closeness of the model to experimental data.

Furthermore, the Nash-Sutcliffe Coefficient of Efficiency (NSE) defined as follows:

$$E = 1 - \frac{\sum_{i=1}^{n}\left(X_{\mathrm{obs},i} - X_{\mathrm{model}}\right)^2}{\sum_{i=1}^{n}\left(X_{\mathrm{obs},i} - \overline{X_{\mathrm{obs}}}\right)^2}, \tag{20}$$

where X_{obs} is observed values and X_{model} is modeled values at time I, is generally used to quantitatively describe the accuracy of model outputs. The closer the model efficiency is to 1, the more accurate the model is. The computed NSE value for the present model efficiency (0.988) confirms that the theoretical formulation proposed here for the roof inner temperature is realistic.

6. Conclusion

The present study has the merit of establishing, for the first time in West Africa, relationships between direct solar radiation at ground level and atmospheric temperature and between atmospheric temperature and indoor temperature. The model that is developed will be of great interest to tropical buildings designers, climate engineers, and anyone interested in indoor comfort cost-benefit analysis, in the line of global warming. Further studies are underway to test various materials used as roof covers in sub-Saharan region of Africa.

Acknowledgments

The authors are thankful to la Cooperation Francaise for the partial support to this study and the former Ecole Inter

Etats des Ingenieurs de l'Equipement Rural for providing the comfortable working environment.

References

[1] J. M. Jahi, K. Aiyub, K. Arifin, and A. Awang, "Human habitat and environmental change: from cave dwellings to megacities," *European Journal of Scientific Research*, vol. 32, no. 3, pp. 381–390, 2009.

[2] *GRET Toitures en Zones Tropicales Arides*, vol. 1, SOFIAC, Paris, France, 1984.

[3] *GRET Bioclimatisme en Zone Tropicale: Construire avec le Climat*, SOFIAC, Paris, France, 1986.

[4] M. Ueda, "Roof types visualisation for human habitats indicator," Department of Computor Software, University of Aizu, (unpublished).

[5] A. E. Obia, H. E. Okon, S. A. Ekum, E. E. Eyo-Ita, and E. A. Ekpeni, "The influence of gas flare particulates and rainfall on the corrosion of galvanized steel roofs in the Niger Delta, Nigeria," *Journal of Environmental Protection*, vol. 2, pp. 1341–1346, 2011.

[6] X. Bai, "Integrating global environmental concerns into urban management: the scale and readiness arguments," *Journal of Industrial Ecology*, vol. 11, no. 2, pp. 15–29, 2007.

[7] K. Veisten, Y. Smyrnova, R. Klæboe, M. Hornikx, M. Mosslemi, and J. Kang, "Valuation of green walls and green roofs as soundscape measures: including monetised amenity values together with noise-attenuation values in a cost-benefit analysis of a green wall affecting courtyards," *International Journal of Environmental Research and Public Health*, vol. 9, no. 11, pp. 3770–3788, 2012.

[8] K. S. Liu, S. L. Hsueh, W. C. Wu, and Y. L. Chen, "A DFuzzy-DAHP decision-making model for evaluating energy-saving design strategies for residential buildings," *Energies*, vol. 5, no. 11, pp. 4462–4480, 2012.

[9] T. Takakura, S. Kitade, and E. Goto, "Cooling effect of greenery cover over a building," *Energy and Buildings*, vol. 31, no. 1, pp. 1–6, 2000.

[10] C. Y. Jim, "Green-space preservation and allocation for sustainable greening of compact cities," *Cities*, vol. 21, no. 4, pp. 311–320, 2004.

[11] C. Y. Jim, "Ecological design of sky woodland in compact urban Hong Kong," in *Greening Rooftops for Sustainable Communities*, pp. 1–15, Green Roofs for Healthy Cities, Baltimore, Md, USA, 2008.

[12] R. A. Romero, G. Bojórquez, M. Corral, and R. Gallegos, "Energy and the occupant's thermal perception of low-income dwellings in hot-dry climate: Mexicali, México," *Renewable Energy*, vol. 49, pp. 267–270, 2013.

[13] G. Baird and C. Field, "Thermal comfort conditions in sustainable buildings—results of a worldwide survey of users' perceptions," *Renewable Energy*, vol. 49, pp. 44–47, 2013.

[14] K. M. Al-Obaidi, M. Ismail, and A. M. Abdul Rahman, "An innovative roofing system for tropical building interiors: separating heat from useful visible light," *International Journal of Energy and Environment*, vol. 4, no. 1, pp. 103–116, 2013.

[15] Z. Dostál, M. Bobek, and J. Župa, "The measuring of global solar radiance," *Acta Montanistica Slovaca*, vol. 13, no. 3, p. 357, 2008.

[16] M. S. Okundamiya and A. N. Nzeako, "Estimation of diffuse solar radiation for selected cities in Nigeria," *IRSN Renewable Energy*, vol. 2011, Article ID 439410, 6 pages, 2011.

[17] S. Awasthi and P. Mor, "Web based measurement system for solar radiation," *International Journal of Advanced Computer Research*, vol. 2, no. 4, pp. 2277–7970, 2012.

[18] K. C. K. Vijaykumar, P. S. S. Srinivasan, and S. Dhandapani, "A performance of hollow clay tile (HCT) laid reinforced cement concrete (RCC) roof for tropical summer climates," *Energy and Buildings*, vol. 39, no. 8, pp. 886–892, 2007.

[19] L. L. Bayala, *Monographie de la Ville de Ouagadougou*, Ministere de l'Economie, 2009.

[20] S. Keevallik and K. Loitjärv, "Solar radiation at the surface in the Baltic Proper," *Oceanologia*, vol. 52, no. 4, pp. 583–597, 2010.

[21] J. A. Duffie, *Solar Engineering of Thermal Processes*, John Willey & Sons, New York, NY, USA, 1980.

[22] F. Kreith and J. F. Kreider, *Principles of Solar Engineering*, Hemisphere Publishing, New York, NY, USA, 1978.

[23] S. I. Khan and A. Islam, "Performance analysis of solar water heater," *Smart Grid and Renewable Energy*, vol. 2, pp. 396–398, 2011.

[24] V. H. Hernandez-Gomez, J. J. Contreras Espinosa, D. Morillon-Galvez, J. L. Fernandez-Zayas, and G. Gonzalez-Ortiz, "Analytical model to describe the thermal behavior of a heat discharge system in roofs," *Ingeniera Investigacion y Tecnologia*, vol. 3, no. 1, pp. 33–42, 2012.

[25] F. Motte, G. Notton, C. Cristofari, and J.-L. Canaletti, "A building integrated solar collector: performances characterization and first stage of numerical calculation," *Renewable Energy*, vol. 49, pp. 1–5, 2013.

[26] C. Yousif, G. O. Quecedo, and J. B. Santos, "Comparison of solar radiation in Marsaxlokk, Malta and Valladolid, Spain," *Renewable Energy*, vol. 49, pp. 203–206, 2013.

[27] R. L. Doneker, T. Sanders, A. Ramachandran, K. Thompson, and F. Opila, "Integrated modeling and remote sensing systems for mixing zone water quality management," in *Proceedings of the 33rd IAHR Congress*, Vancouver, Canada, 2009.

[28] M. Benedini and G. Tsakiris, *Model Calibration and Verification*, Printforce, Alphen aan den Rijn, The Netherlands, 2013.